



HAL
open science

On the possibility of ultrafast KOSSEL diffraction

Olivier Peyrusse

► **To cite this version:**

Olivier Peyrusse. On the possibility of ultrafast KOSSEL diffraction. *Matter and Radiation at Extremes*, 2022. hal-03697979

HAL Id: hal-03697979

<https://amu.hal.science/hal-03697979>

Submitted on 17 Jun 2022

HAL is a multi-disciplinary open access archive for the deposit and dissemination of scientific research documents, whether they are published or not. The documents may come from teaching and research institutions in France or abroad, or from public or private research centers.

L'archive ouverte pluridisciplinaire **HAL**, est destinée au dépôt et à la diffusion de documents scientifiques de niveau recherche, publiés ou non, émanant des établissements d'enseignement et de recherche français ou étrangers, des laboratoires publics ou privés.

On the possibility of ultrafast KOSSEL diffraction

Olivier Peyrusse¹

Aix-Marseille Université, CNRS, Laboratoire LP3, UMR7341, 13288 Marseille, France.

(*Electronic mail: olivier.peyrusse@univ-amu.fr)

(Dated: 5 May 2022)

We discuss the possibility of realizing time-resolved Kossel diffraction experiments for providing indications on the crystalline order or on the periodic structure of a material. We make use of the interaction of a short, ultra-intense laser pulses with a solid target which generates short bursts of hot electrons. Penetrating inside a layered sample (i.e. a crystal or an artificial multi-layer material), these electrons ionize inner-shell electrons so that the subsequent radiative filling of K-shell vacancies results in a strong $K\alpha$ emission which is enhanced in the Bragg directions corresponding to the period of the material. We present simulations of the angle-resolved $K\alpha$ emission which displays the so-called Kossel patterns around the Bragg angles. Then, we discuss possible experiments appropriate for laser facilities delivering short and intense pulses.

Keywords: x-ray emission, Kossel diffraction, ultra-intense lasers

I. INTRODUCTION

Very quickly after their discovery x-rays have been used for obtaining structural information on solid density matter. In particular, x-ray crystallography is a well-established tool for measuring time-averaged positions of atoms in periodic systems. More recently, x-ray-based investigations focused on the phase-transition dynamics using diffraction (for a review see Ref. 1) and using time-resolved X-ray absorption near-edge spectroscopy (for a review see Ref. 2). What is sought in this context, is a measurement of the change in the spatial arrangement of atoms on the pathway leading to a structural change. Typically, the timescale of interest is between 10^{-14} and 10^{-12} s. For these studies, a natural approach is the femtosecond x-ray crystallography.³⁻⁸ A first requirement for this approach is a source of femtosecond x-ray pulses. Among these sources, $K\alpha$ emission driven by table-top, short, intense and high-repetition laser sources has proven to be convenient (see Refs. 9 and 10 and references therein). These x-ray $K\alpha$ emission sources result from inner-shell ionization by the hot electrons generated by the interaction of short, ultra-intense laser pulses with solid matter. Then, one exploits these short $K\alpha$ x-ray bursts for probing matter (using x-ray diffraction) in pump-probe experiments where an external pump (most often another pulse of low intensity but from the same laser chain to avoid any uncontrolled jitter) drives a macroscopic excitation of the sample. In this context, these sources have been shown to be efficient in experiments requiring a 100 fs time resolution.¹¹ These studies do not pay further attention to the possible specificities of K-shell emission where it is just a way to obtain x-ray photons to be diffracted by a sample. Here, one remarks that in itself, K-shell emission spectroscopy may be a useful structural tool. For instance, $K\beta$ spectroscopy gives information in 3d transition metal systems¹² (although indirectly through the interaction between 3p holes and 3d electrons). We note here that change in the spectral features of $K\alpha, \beta$ lines due to the chemical environment requires high spectral resolution ($\lambda/\Delta\lambda \geq 5000$). Another remark is that, if x-ray emission takes place inside a crystal, outgoing emission is strongly enhanced in directions located on the surface of a cone of semi-angle $\frac{\pi}{2} - \theta_B$ (θ_B being the Bragg angle) and of axis normal to the hkl planes of the crystal. This angular distribution of x-ray emission is known as Kossel diffraction¹³ or *x-ray standing wave at reverse*.¹⁴ In the vicinity of these cones, the intensity variation leads to characteristic Kossel angular profiles. Compared with traditional x-ray diffraction, it is known that these profiles contain also an information on the phase¹⁵⁻¹⁷ which is a unique aspect of Kossel diffraction. In itself, this unique aspect justifies a careful analysis of Kossel diffraction possibilities for

the study of fast-evolving dense matter samples. This may have an impact on studies concerning extreme states of matter. One notes however that the task for a quantitative analysis of Kossel line profile is very involved and that before this, one has to discuss the possibility of observing and measuring these profiles in transient conditions, which is the goal of this article.

According to these remarks, the idea developed in this paper is the following: why not directly use the information brought by $K\alpha$ emission arising in a periodic structure, as it results from the burst of hot electrons produced by the interaction of a short, high-intensity laser pulse with matter. In other words, the idea is to use the hot electron flux arising from a target submitted to a high-contrast, high-intensity, ultra-short laser and then, analyze the spatial structure of $K\alpha$ emission arising from a prepared sample submitted to this electron flux. The interest of this approach could be an access to in depth structural modifications compared with X-ray diffraction based on reflectivity measurements. This raises the question of the material heating by the hot electron flux itself. This heating results, in a first step - from the collisional thermalization of these hot electrons and in a second step - from the coupling of the thermal electron bath with the lattice. Impact of the last coupling in term of structural modifications is felt typically after 1 ps so the duration of the hot electron burst (inducing the $K\alpha$ burst) must be much smaller than 1 ps, i.e. typically a few tens of fs. Duration of this burst (the probe) gives also the possible time-resolution expected in experiments where some information is sought concerning the structural dynamics of a material heated by some external means (the pump). We remark here that the thermal electron temperature increasing due to the hot electron energy deposition is not an issue in pump-probe experiments where a sub μm sample is refreshed after each shot. In other word, whatever its intrinsic perturbation, the hot electron burst (starting at t) remains a probe of about 100 fs duration at maximum (this includes pulse duration, propagation and $K\alpha$ emission) in a thin material previously prepared by the pump (at $t - \Delta t$, where Δt is a variable delay). As explained below, Kossel diffraction lines are a signature of a layered structure whether it is natural (crystals) or artificial (stack of nm thick layers of different materials). We discuss here some specificities of the fluorescence emission from such media, as resulting from the inner shell excitation by a short burst of hot electrons. In the case of crystals, and at the wavelength of the fluorescence lines, an appropriate angular scan around the Bragg angle should give a clear indication of the crystalline order. As said above, if the medium is by some mean heated in a controlled manner (pump-probe experiments), the disparition of the Kossel structures is a clear indication of the loss of crystalline order. By using different delays between the pump and the short burst of electrons, this loss of crystalline order could be followed

in time. Below the melting temperature (low fluence pump excitation), there is also the possibility to study the modification of Kossel patterns as a function of time (to follow the strain propagation for instance). In this article, we discuss also the potentiality of detecting Kossel structures from artificial multilayers or detecting specific phonons resulting from a specific excitation in solids. Again, we remind that, since the inner-shell ionization can be provided in depth, this analysis might be applied to specific samples embedded in another material. Finally, many conclusions in this article apply also to the case where the ionization source is a short and intense photon source such an x-ray free-electron laser (XFEL) where (inner-shell) collisional ionization is replaced by photoionization.

To complete this introduction, it is important to notice that Kossel diffraction is just one aspect among other specificities of "inside" sources emission. Indeed, considering individual atoms in a large periodic structure, the intensity of radiation coming from one particular atom can be formally written in first Born approximation as^{18,19} $I(\vec{k}) = |R(\vec{k})|^2 + \sum_i R(\vec{k})S_i(\vec{k}) + \sum_{i,j} S_i(\vec{k})S_j(\vec{k})$ where \vec{k} is the emission wave-vector. R is the electric wave-field of the radiating atom, S_i is the wave scattered by atom i , summations being carried over all atoms except the emitter. The first term represents the emission of the atom itself. It is angle independent (at least if one neglects reabsorption) and represents a constant background. For objects with a long-range order (crystals) and considering many radiating atoms, interferences of secondary waves (the third term) leads to the Kossel patterns. The second term which is responsible of a weak angle modulation of the intensity (between and below the Kossel patterns) contains some *holographic* information concerning the neighborhood of the radiating atom. The possibility of extracting holographic information from this term was first mentioned by Szöke.²⁰ It is possible^{19,21,22} but technically complicated and time-consuming (for a review, see for instance Ref. 23). In the present article, we do not consider the weak angle modulation associated with this holographic component of the "inside" emission of atoms.

II. KOSSEL DIFFRACTION IN LAYERED MEDIA IRRADIATED BY HOT ELECTRONS

The so-called Kossel diffraction corresponds to x-ray interferences from lattice sources. These interferences cause a modulation of the x-ray line intensity as a function of the exit angle. This phenomenon was predicted by W. Kossel²⁴ and first observed later¹³ from the fluorescence fol-

lowing electron excitation of a copper single crystal. In addition to electrons, this excitation can be accomplished by protons or by x-rays, each atom in the lattice becoming the origin of a spherical wave interfering with others. Modulation of the outgoing fluorescence intensity arises in a narrow angular range around θ_B satisfying the Bragg condition $d^{sample} \sin \theta_B = n\lambda^{sample}/2$. d^{sample} is the interreticular distance in the crystal while λ^{sample} is the wavelength of the fluorescence line (typically a $K\alpha$ line). One sees that λ^{sample} must be smaller than $2d^{sample}$ so that not all the crystals can display Kossel lines. This is the case for Mg, Al or Si for instance. As said above, another consequence is that x-ray emission is distributed on the surface of a cone of semi-angle $\frac{\pi}{2} - \theta_B$, and on an axis normal to each reticular plane hkl .¹⁴

Kossel diffraction have different applications. Among them, we note, lattice constants determination, crystal orientation, residual stress measurements in the micro-range or phase transformation in the high- or low-temperature range (see²⁵ and references therein). In artificial multilayer materials (stack of nm-size layers of different materials) dedicated to x-ray optics, Kossel patterns in the x-ray fluorescence following photon²⁶ and electron^{27,28} excitation, have also been observed and interpreted (for a review, see Ref. 29). In these studies, the goal was to obtain information on the interfacial roughness and interdiffusion from Kossel line features. Still for layered media, recent calculations of these patterns focused on the case of strong photon excitation such as provided by XFEL irradiation.³⁰ In this article, we will consider only multilayers defined as a stack of bilayers and denoted as $(Z_1/Z_2)_N$ where Z_i is the element of medium i (which can be the vacuum as explained below) and N is the total number of bilayers. Further, one defines the thickness of medium 1 as e_1 , the thickness of medium 2 as e_2 and the period as $d = e_1 + e_2$.

A. Modeling of the physical processes

1. Fluorescence emission

For calculating the Bragg diffraction of the fluorescence emission inside a 1D multilayer, we use the model described in Ref. 19, the only difference being in the ionization which is provided here by a short burst of hot electrons instead of photons. The slowing-down of these electrons provide an in-depth distribution of ionization which is not homogeneous. Modeling of this distribution relies on a model of hot electron transport to be described in the next subsection. For a

crystal, we consider the simple picture where the 3D lattice is replaced by a layered lattice. The material is supposed to be distributed uniformly in the lattice planes parallel to the surface. In other word, the crystal is approximated by a stack of bilayers of period d (the reticular distance between 2 planes) where the first layer is the layer of atoms while the second layer is an empty layer of refractive index 1. While being a rough method to simulate the problem of the distribution of individual small scatterers, the replacement of real atoms by a uniform layer of a given thickness e_1 , has a semi-empirical validity. A relevant quantity to measure its effectiveness is the reflectivity which for a wavelength of interest can be calculated around the Bragg angle and compared with a model giving the reflectivity of a real crystal. Such models are based on the dynamical x-ray diffraction theory (for a recent review of modern implementations, see for instance Ref. 31). As in Ref. 30, calculations of the electric field in this article are based on a solution of the Helmholtz equation applied to materials defined as a juxtaposition of media of different indices. Then, x-ray reflectivity of a crystal can be obtained from a solution of the one-dimensional Helmholtz equation applied to the stack (element/vacuum) $_N$. We compared such reflectivities with results of the XOP-SHADOW package^{32,33} allowing a calculation of the reflectivity in real crystals. We found that, taking for the element thickness a typical value of $e_1 = 0.4d$ (d being the proper inter-reticular distance in the crystal of interest) and renormalizing properly the number of atoms in this element layer to the right number of atoms (per volume unit), this approach gives results close to more realistic crystals models. As an example, Figure 1 displays the rocking curve of a Ge 111 sample for 3 different thicknesses, around the Bragg angle and for an incident photon energy corresponding to the Cu $K\alpha$ line (8047.8 eV). A comparison is made between our approach and results from the XOP-SHADOW package.^{32,33} The match is not perfect but one can see that our simplified 1D approach gives satisfactory results concerning the width and the shape of the diffraction pattern. For the following, the interest of our approach is that it allows for a comprehensive modeling of both the fluorescence and of the hot electron transport in a layered medium whose a crystal is an example.

As in Ref. 30, the fluorescent field $E(z, \theta)$ in each point of the multilayer and arising on the detector is calculated by solving the Helmholtz wave equation and by invoking the reciprocity theorem,^{34,35} i.e. by considering a fictitious source located at infinity and emitting at the fluorescence line wavelength. Fluorescence intensity at infinity away from the sample and function of the exit angle θ is then $I = \int j(z)|E(z, \theta)|^2 dz$ where $j(z)$ is the fluorescence emissivity induced locally by inner-shell ionization. $j(z)$ is proportional to the upper level population of the fluores-

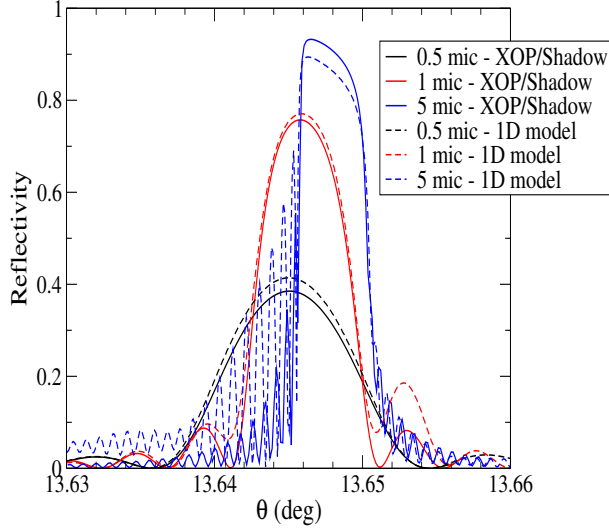


FIG. 1. Rocking curve of Ge 111 samples of different thicknesses around the Bragg angles at 8047.8 eV. Plain lines correspond to calculations based on the standard methods of the XOP package,^{32,33} dashes: present 1D model as discussed in the text.

cent transition and to the corresponding Einstein coefficient. A basic ingredient for the Helmholtz wave-equation is the local complex refractive index whose real and imaginary parts depend on the distribution of atomic populations in the multilayer (see Ref. 30 for more details). Here, this distribution is linked to the local distribution of the free electrons (thermal and hot electrons) driving the ionization.

2. *K-shell ionization and fast electron transport*

For calculating the fast electron transport, we used a 1D deterministic model developed for calculating the transport of high-energy photoelectrons as produced in the interaction of multikeV photons with matter.³⁶ The right terms of the standard transport equation for the angular fluence of hot electrons (denoted W) are a source term Q and a collision operator $C(W)$ accounting for slowing-down and scattering in other directions (see Ref. 36 for more details). This collision operator is written at the Fokker-Planck approximation.³⁷ It is important to note that the model is 1D in the sense that it applies to the propagation of electrons in a medium stratified in parallel plane perpendicular to the z -axis. According to this axis, different discretized propagation directions $\mu_i = \cos \theta_i$ are considered so that each electron (or rather each group of electrons) may be scattered locally in a different direction, at each time step. Therefore, both the local fluence

W and the source term Q depend on the four quantities E, z, t, μ so that $Q(E, z, t, \mu)$ is a number of hot electrons of energy E produced per interval of energy ΔE , at position z , at time t and of traveling direction μ . For simplicity, this source is put on one side of the medium (the outermost cell) and is supposed to follow the laser deposition of energy on hot electrons so that Q has the form $Q(kT_h, z_b, t, \mu_n) = Q_o \exp(-(t - t_o)^2 / \tau_L^2)$ where τ_L is the duration of the laser pulse and t_o indicates the peak of the pulse. kT_h is the typical energy of hot electrons, z_b is the boundary of the medium and μ_n is the normal direction. Also, one takes $Q_o = \frac{\eta I_L}{kT_h} \frac{1}{dz \Delta E}$ in which dz is the thickness of the outermost cell, ΔE is the energy bin, I_L is the laser fluence and η is the conversion efficiency of laser light into hot electrons. Because hot electrons considered here are of much higher energy than XFEL-induced photoelectrons, we added to the electron collisional stopping power³⁸ present in $C(W)$ a *collective* (or *resistive*) contribution due the return current generated by thermal free electrons in response to the hot electron current (see Ref. 39 and references therein). Note that we are interested here in electron propagation and not in electron generation so that initial values of the hot electron energy kT_h and of the conversion efficiency η of laser light into hot electrons, are obtained from well-known I_L -dependent scaling laws, i.e. the Wilks scaling law⁴⁰ as corrected by Sherlock⁴¹ and the Yu's scaling law,⁴² respectively. Finally, an important quantity driving the population of the core-ionized atoms responsible of the $K\alpha$ emission is the local K-shell ionization rate $2\pi \int d\mu \int dE W(E, z, t, \mu) \sigma_K(E)$ where σ_K is the K-shell ionization cross-section. This rate enters the collisional-radiative system driving the atomic populations which has to be solved locally along with the transport equation (see Ref. 36 for more details). There are many theoretical and empirical expressions for σ_K (for a review, see Ref. 43). Hombourger's one⁴⁴ has been used in this paper. Note that the energy range of the hot electrons requires the use of the Grynski's relativistic factor which contains typing errors in Ref. 44 (see Ref. 43 for the correction). Finally, it is important to keep in mind that validity of this 1D approach is *a priori* restricted to situations where the sample thickness is smaller than the size of the focal spot. Results are just informative in the opposite case.

III. SIMULATION RESULTS

A. Hot electron energy deposition in a Ni crystal - $K\alpha$ Fluorescence

An example of simulation of hot electron energy deposition (consequence of the hot electron transport) in a $1\ \mu\text{m}$ thick Ni sample is displayed in Fig. 2. Here the laser pulse is of 20 fs duration, of intensity $1.3\ 10^{18}\ \text{W}/\text{cm}^2$ at the wavelength 800 nm. According to the Yu's law,⁴² the conversion efficiency in hot electrons is $\eta = 0.046$. In these conditions, the typical energy of these hot electrons is $kT_h = 50\ \text{keV}$. In Fig. 2 are plotted the spatial profiles of the thermal electron temperature for different instants during the pulse. Note that the hot electron beam comes from the right. This thermal electron temperature is supposed to transfer to the lattice but on a time scale much larger than the hot electron pulse duration. Then, over its own time duration, the structural information carried by the $K\alpha$ emission is not impacted by this hot electron heating in a single shot mode. As resulting from the inner-shell ionization by hot electrons, the Ni $K\alpha_1$ emission (7478.15 eV) at different times during the pulse, is displayed in Fig 3. More precisely, what is shown in Fig. 3 is an angular scan of the $K\alpha_1$ emission in the front side of the sample (i.e. the right side), θ being the observation angle relative to the surface of the sample. In these calculations, (111) planes of Ni are assumed parallel to the surface so that our $1\ \mu\text{m}$ thick Ni crystal is approximated by a stack of 4630 bilayers of period $d = 0.216\ \text{nm}$ where the first layer (of thickness $e_1 = 0.4d$, see Sec.II.A.1) is a layer of Ni atoms while the second layer is empty. Also, this emission corresponds here to the emission associated with all ionization stages compatible with the "cold" valence of Ni.

As discussed above, one observes a strong modulation of the outgoing emission around the Bragg angle $\theta_B = 22.6^\circ$. Note that for an irradiation of the sample by hot electrons of higher energy and intensity, the result is not really different (except for the signal intensity). This is shown in Figure 4 which corresponds to the fluorescence resulting from hot electron excitation following the interaction by a laser pulse of 20 fs duration, but of intensity $10^{19}\ \text{W}/\text{cm}^2$. Here the conversion efficiency is $\eta = 0.21$ and the typical energy of hot electrons is $kT_h = 450\ \text{keV}$. The inset is a zoom of the Kossel structure for the time of maximum emission. Also shown is the final profile (dotted line) obtained by convolution by a gaussian profile of width related to the angular broadening due to the energy width of the $K\alpha$ line. Indeed, a simple differentiation of the Bragg relation gives $\Delta\theta = (\frac{\Delta E}{E}) \tan \theta$. From a reported FWHM measurement⁴⁵ of the Ni $K\alpha_1$ line ($\Delta E = 2.25\text{eV}$) we get $\Delta\theta = 7\ 10^{-3}\ \text{deg}$. Note that, after a few tens of fs, this intrinsic broadening

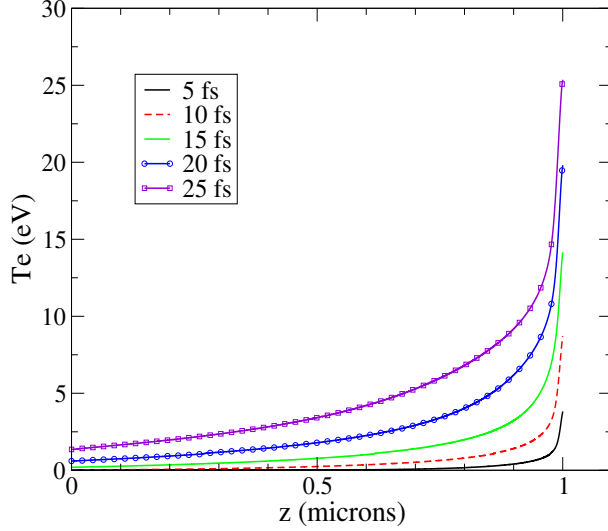


FIG. 2. Snapshots at different times of the thermal electron temperature in a 1 μm thick Ni foil. The hot electron beam comes from the right. Parameters of the simulation are given in the text.

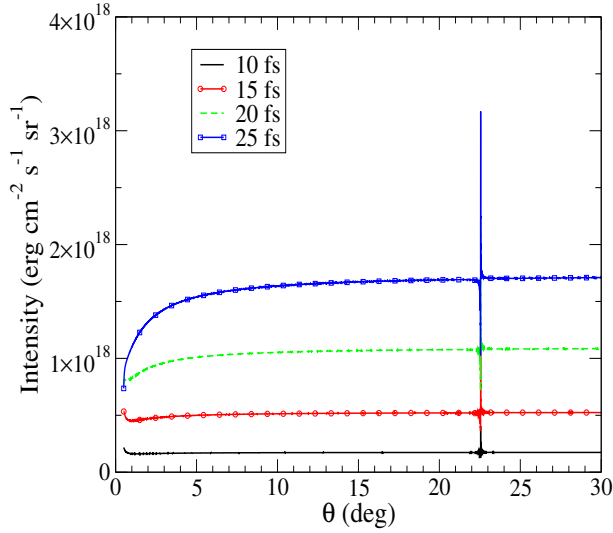


FIG. 3. Snapshots at different times of the $K\alpha_1$ emission from a Ni sample as a function of the observation angle. Parameters of the simulation correspond to Fig. 2.

in likely to be increased by the ionization and thus limiting in time the observability of the Kossel structure. In a way, this reinforces the ultra-fast aspect of the Kossel signature in these conditions. There is also another contribution to the angular broadening which is purely geometric and due to the size of the emitting source. As discussed below in Sec. IV, this contribution can be made negligible. Structures shown in Figs 3-4 are typical of the crystalline order of the material hosting the emission. These features are likely to fade away with ion temperature and to disappear when

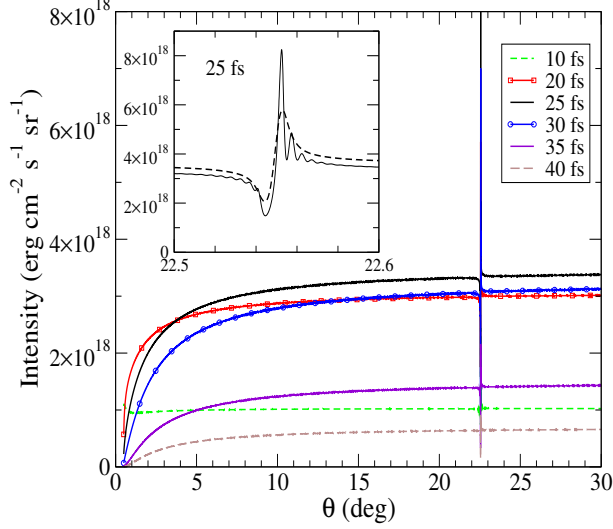


FIG. 4. Snapshots at different times of the $K\alpha_1$ emission from a Ni sample as a function of the observation angle. Parameters of the simulation are given in the text. The inset is a zoom of the emission for the time of maximum emission. Dotted line is the broadened profile when one takes into account the FWHM energy broadening of the $K\alpha_1$ line.

atomic displacements reach about 10% of the mean nearest-neighbour distance, i.e. when the crystal undergoes a solid-to-liquid phase transition (Lindemann criterion). However, this behavior can hardly be studied with our one-dimensional approach.

To finish this paragraph concerning Ni $K\alpha$ fluorescence, we present in Fig. 5, the $K\alpha$ fluorescence around the Bragg angle for a thin film (100 nm) of Ni. Irradiations conditions correspond to Fig. 3, i.e. a gaussian pulse of intensity $1.3 \cdot 10^{18}$ W/cm² and of duration 20 fs (wavelength 800 nm). Shown are three snapshots of Kossel patterns around and at the peak of emission (23 fs). Here modulations are broader, of lower absolute intensity since the number of emitting atoms is less. However, as we will see in Section IV, this level of intensity remains detectable.

B. Hot electron energy deposition and $K\alpha$ fluorescence in a Mo crystal

Here, we present calculations concerning another material, namely molybdenum. (111) planes of Mo are supposed to be parallel to the surface of a 1μ thick sample. The crystal is then approximated by a stack of 5504 bilayers of period $d = 0.1817$ nm (the inter-reticular distance) where (for solving the Helmholtz equation) the first layer of thickness $e_1 = 0.4d$ (see Sec.II.A.1) is a layer of Mo atoms while the second layer is empty. Irradiation conditions correspond to Fig. 5, i.e. a gaus-

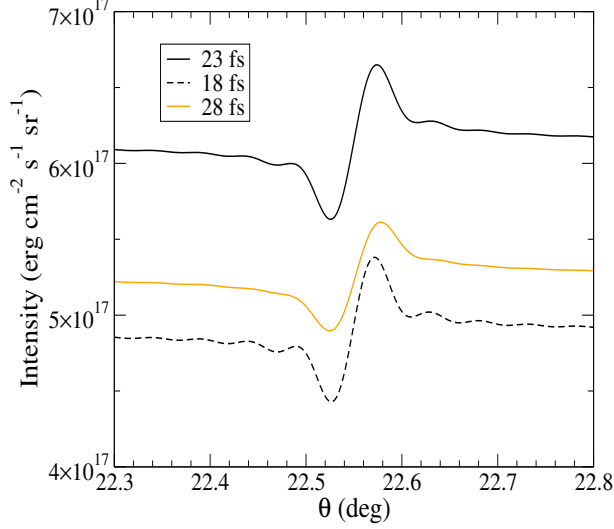


FIG. 5. Kossel patterns at different times of the $K\alpha$ emission from a 100 nm thick Ni sample. Irradiation parameters of the simulation are those of Fig. 3.

sian pulse of intensity 10^{19} W/cm² and of duration 20 fs. A few snapshots of the $K\alpha_1$ (17479.34 eV) angular emission are displayed in Fig. 6. The inset is a zoom of the Kossel structure around $\theta_B = 11.25^\circ$, at the peak of emission. Again, dashed curve shows the final profile obtained by convolution by a gaussian profile of angular width $\Delta\theta = 4 \cdot 10^{-3}$ deg related to the energy width ($\Delta E = 6.38$ eV) of the Mo $K\alpha_1$ line.⁴⁶

C. $K\alpha$ fluorescence from a multilayer

Instead of a natural crystal, one considers here an artificial multilayer material in which a fluorescence $K\alpha$ emission is induced by hot electron ionization. The material studied here is a stack of 125 bilayers (Mg/Co) of thicknesses $e_1 = 5.45$ nm and $e_2 = 2.45$ nm, respectively. The period is then $d = 8$ nm for a total thickness of 1 μ m. We applied the methods discussed in Sec. II for calculating the Mg $K\alpha$ fluorescence (1253.6 eV) as a function of the exit angle θ . The hot electron source corresponds to a laser pulse of 20 fs duration, of intensity $1.3 \cdot 10^{17}$ W/cm² at the wavelength 800 nm so that the conversion efficiency in hot electrons is $\eta = 0.008$ and the typical energy of hot electrons is $kT_h = 16$ keV. Figure 7 displays a few snapshots of the angle-resolved $K\alpha$ emission. One observes the specific Kossel patterns for the different Bragg angles of the multilayer. Compared with a pure crystal, the modulations are broader. Note that such patterns are likely to be affected by the roughness of interfaces. Introducing the roughness in the calculations

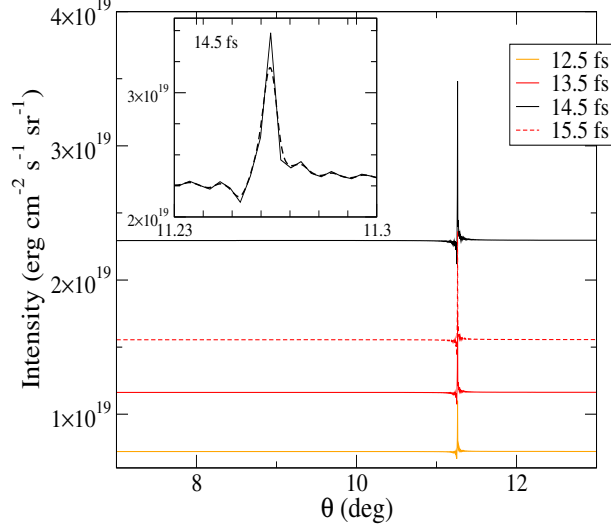


FIG. 6. Snapshots at different times of the $K\alpha_1$ emission from a Mo sample as a function of the observation angle. Parameters of the simulation are given in the text. The inset is a zoom of the emission for the time of maximum emission. Dotted line is the broadened profile when one takes into account the FWHM energy broadening of the $K\alpha_1$ line.

and fitting the Kossel features is a way to characterize the quality a multilayer.²⁹

D. Effect of vibrational dynamics on Kossel structures

It has been shown that the absorption of a near infra-red laser pulse with a duration of about 100 fs may provide a coherent excitation of longitudinal phonons with a large amplitude.^{4,7,8,47} Considering that this phonon excitation corresponds to coherent oscillations of atomic planes about their equilibrium positions, we modeled such oscillations in a 400 nm thick Ni film while it is submitted to a hot electron beam providing inner-shell ionization. In our approach, this means that the displacement of each Ni layer k around its equilibrium position x_k is $\epsilon_k = Ad \cos(kx_k - 2\pi\nu(k)t)$ where A is the amplitude of the displacement and d is the proper inter-reticular distance. $k = \xi \frac{\pi}{d}$ is the phonon wave-vector defined in term of the *reduced wave-vector* ξ while the frequency $\nu(k)$ obeys a dispersion relation. From Ref. 48 and for a reduced wave-vector of 1, the measured longitudinal phonon dispersion curve along the 111 direction of Ni (where $d = 0.216$ nm) gives a frequency $\nu = 9 \cdot 10^{12}$ Hz. Figure 8 displays typical snapshots of the angle-resolved $K\alpha$ emission at different times during this particular oscillation where the amplitude A has been set to 10%. Here we assumed that our Ni film is homogeneously excited. In figure 8, one can observe how

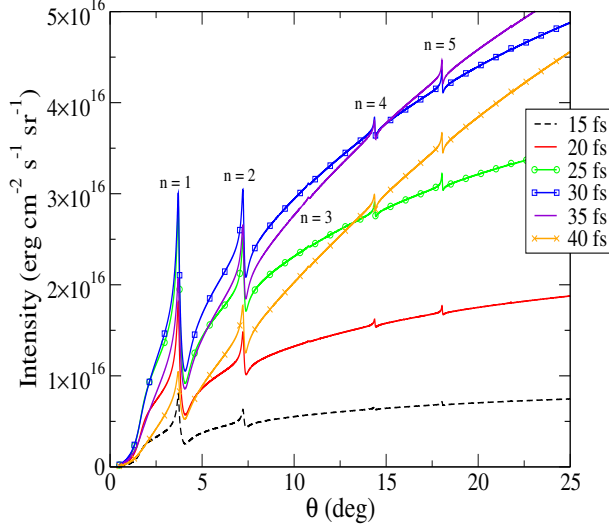


FIG. 7. Snapshots at different times of the Mg $K\alpha$ emission from a $1 \mu\text{m}$ thick multilayer $(\text{Mg}/\text{Co})_{125}$ as a function of the observation angle. Parameters of the simulation are given in the text. Kossel patterns are labeled by their Bragg order.

the phonon oscillation results in an oscillation of the Kossel structure. One can notice that a more heavier crystal material than Ni would exhibit smaller frequency oscillations. Such oscillations could more easily be probed by short bursts (a few tens of fs or less) of hot electrons. Likewise, the propagation of acoustic waves (superposition of longitudinal phonons in the subterahertz range) is likely to provide more pronounced oscillations of a Kossel structure around the Bragg angle as does a standard diffraction pattern.⁴⁹

We note that nanostructures which consist in a stack of nm thick crystalline layers as considered in III.C, may exhibit also coherent vibrations: the so-called super-lattice (SL) vibrations.⁸ These SL vibrations could also be probed by Kossel diffraction.

IV. ULTRA-FAST STRUCTURAL DYNAMICS WITH A PUMP-PROBE APPROACH - TYPICAL EXPERIMENTAL CONFIGURATIONS

A presentation of mechanisms exciting motion lattice in different materials is beyond the scope of this article (for a review see Ref. 50) and likewise the generation of coherent plasmons at THz frequencies. Here we restrict ourselves to a few remarks concerning transient effects between electron and lattice temperatures in a metal or in a semi-conductor, after excitation by an ultrashort laser (the so-called *pump*). There is indeed a great interest in understanding these electron-ion

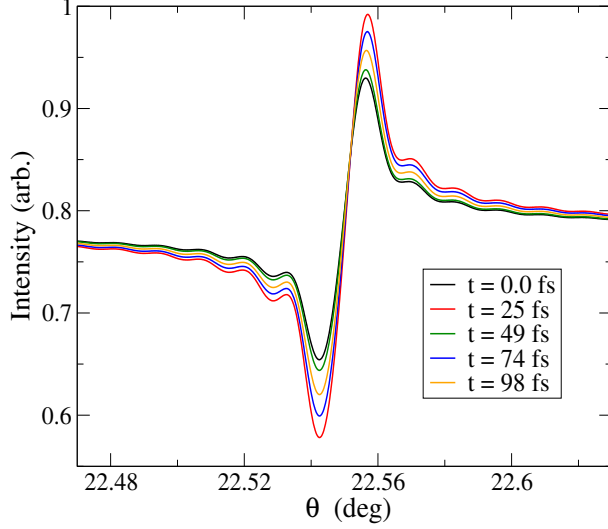


FIG. 8. Snapshots at different times during a phonon oscillation, of the $K\alpha$ emission from a 400 nm thick Ni sample as a function of the observation angle around the Bragg angle. Parameters of the simulation are discussed in the text.

dynamics interplay in this context. First, one has a fast deposition of the laser energy (pump) onto free electrons which thermalizes very-quickly into a hot (quasi-Fermi) distribution. Then starts an energy transfer to the lattice via electron-phonon couplings. If this transfer (cooling) is fast compared with a phonon oscillation period, the resulting impulsive stress induces long-wavelength acoustic excitations (low-frequency phonons). Resulting strain waves (which can be regarded as a superposition of longitudinal acoustic phonons) are induced by a relaxation of the local pressure induced by the ion excitation and by the electron excitation itself. In x-ray diffraction measurements, this strain propagation into the lattice induces an oscillation of the diffraction signal around the Bragg angle.⁴⁹ Thus, one remarks that there is no reason why a Kossel pattern would not have the same behavior as a standard diffraction one, i.e. exhibiting an oscillation around the Bragg angle. By this means, one of the issues that is actively studied is the ultrafast heating and cooling of thin (between a few and a few tens nm thick) metallic films as long as the lattice temperature T_i remains less than T_m , the melting temperature, see for instance Ref. 51). Because a strain can be converted into a change of the lattice temperature T_i , x-ray diffraction (but also Kossel diffraction) offers a way to study the thermal transport in a layer stacking of different metals.

Another actively studied issue concerns the ultrafast transition from solid to liquid in metals. One generally assumes that melting occurs when T_i exceeds T_m . Typically when $T_i \geq 1.4 T_m$, lattice disorders within a few vibrational periods. In this context of strong electron excitation

by the pump (well before any probe), there are issues concerning the lattice dynamics for which theoretical calculations predict different behaviors which depends on the nature of the electronic Density-Of-States (DOS). Indeed, the strongly excited electron system can cause a strengthening (bond hardening) or a weakening (bond softening).^{52,53} Concerning hardening (i.e. an increasing of T_m), this effect is predicted to be effective if $T_e \geq 3$ eV in Cu and $T_e \geq 6$ eV in gold where one can expect a factor 3 on T_m . One notes in passing that calculating the evolution of subsystems (electron and ions) requires parameters like, heat capacities C_e , C_i and the electron-ion coupling factor G . These parameters have to be calculated as a function of T_e .⁵⁴ Observing hardening (i.e. an increasing of T_m) requires a probing of the lattice stability on a time shorter than the equilibration between excited electrons and the lattice. Observation of the behavior of Kossel patterns in this context, at different delays from the pump pulse is likely to provide meaningful informations.

A schematic experimental configuration for studying short Kossel patterns is shown in Figure 9. At a time t_L , a short and intense laser beam (of duration τ_L) interacting with a sample is used to produce a short burst of hot electrons. The bulk of the sample is then submitted to this hot electron flux (roughly of duration τ_L). These electrons will ionize 1s electrons of the sample which will result in a strong $K\alpha$ emission to be analyzed. The structural state of the $K\alpha$ emitting zone can be varied by using another pulse (of much lower intensity but from the same laser chain) providing a controlled heating at a time t_p earlier than t_L . In this way, by varying t_L with respect to t_p , it could be possible to observe the change in the $K\alpha$ fluorescence as a function of the delay between t_p and t_L . Then, by varying the observation angle θ around the Bragg angle, one could observe the typical Kossel patterns. In particular, one expects that these Kossel patterns which are a signature of the crystal order in the material, vary and even disappear with a bulk heating. One notices that this zone of structural change must be kept larger than the zone effectively excited by the hot electrons to be sure that the $K\alpha$ signature reflects the modified zone.

For practical reasons, the experimental set up can be such that the directions of the high intensity laser and of the detected photons are roughly perpendicular (depending on the Bragg angle of the problem). The $K\alpha$ emission must be analyzed with a convenient spectrometer positioned at the peak of the line emission and the intensity is measured as a function of the angle θ . In fact, the resolution of the spectrometer does not need to be very high since the goal is to record the $K\alpha$ photons, i.e. integrated over the line profile. In this setup a variation (indicated by the rotation axis) of the exit angle θ must be allowed around the Bragg angle with an uncertainty of less than about 0.01 deg for a good angular resolution of Kossel structures (in crystals). Here one notice

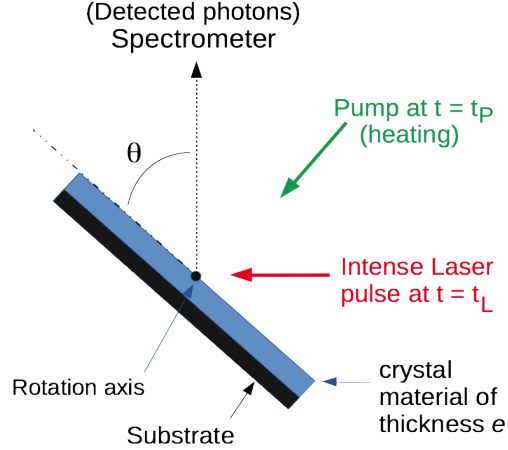


FIG. 9. Geometry of a possible experimental setup for pump-probe Kossel diffraction experiments.

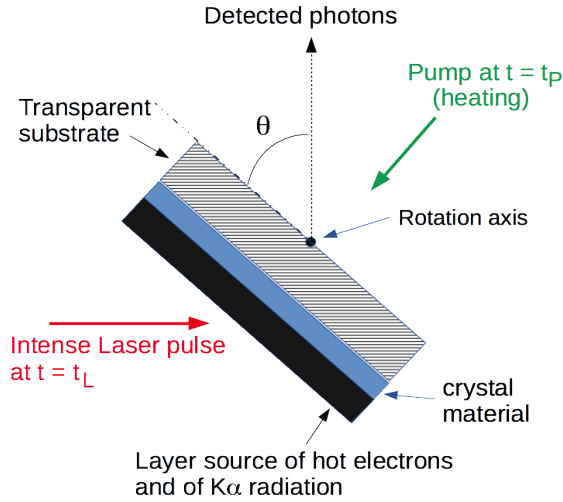


FIG. 10. Another possible experimental setup for pump-probe *Transmission* Kossel diffraction experiments.

that the size of $K\alpha$ emitting zone of the sample lead to a spread of the collected line emission angles over an interval which is just the angle subtended by the emitting zone of diameter D at the detector distance R . This spread leads to a geometrical broadening $\Delta\theta_{geom} = \sin\theta_B \frac{D}{R}$ to be added to the intrinsic broadening $\Delta\theta$ due to the $K\alpha$ line width already discussed in Sec. III-A.

Requirements in term of detection capabilities are the following. Typically, for a $1\mu\text{m}$ thick Ni target, Figure 3 indicates a background $K\alpha$ outgoing intensity of about $1 \times 10^{18} \text{ erg.cm}^{-2}.\text{s}^{-1}.\text{sr}^{-1}$. Taking 7478 eV photons ($K\alpha$), a 20 fs pulse and an expected $K\alpha$ source size of $15 \mu\text{m}$,⁵⁵ one gets a number of 3×10^6 photons emitted per steradian and per shot. For

a thin film, Fig. 5 indicate that about 10^6 $K\alpha$ photons/sr/shot can be expected. These numbers are well above current detection capabilities of typically 10^5 photons/sr/shot⁵⁵ using the photon counting method in which an x-ray CCD camera acts as a dispersive spectrometer.⁵⁶ This detection capability is obtained by accumulating over a few a few hundreds of shots by using a moving target allowing to refresh the interaction zone with the laser, before each shot. Note also that the requirement of a resolution $d\theta$ of about 0.01 deg with a given pixel size s_p for the detector imposes a minimum distance $R = \frac{s_p}{\tan(d\theta)}$ between the detector and the $K\alpha$ emitting zone. For a typical pixel size of 100 μm , the detector should be positioned at $R = 60$ cm. In these conditions the geometric broadening $\Delta\theta_{geom}$ remains negligible compared with the intrinsic broadening $\Delta\theta$ (even with a $K\alpha$ emitting zone much larger than a laser focal spot of a few μm^2). This geometry raises the question of the optimum thickness e of the probed material (see Fig. 9). Indeed, hot electrons produced at its surface must pass through the whole sample while keeping enough energy for K-shell ionizing the sample. While conversion efficiency η and hot electron temperature kT_h do not seem to depend on the Z of the material, transport of these hot electrons does. For a mid- Z element like molybdenum, it is known that hot electrons produced by highly intense laser pulses ($I_L \sim 10^{19}$ W/cm²) do not go over about 4 μm ⁵⁵ (and probably less than that) due to the collective effects mentioned above (Sec. II.A.2). Lighter elements are likely to be more easily crossed by hot electrons. On the other hand, a desirable uniform heating of the sample by the pump laser precludes a thickness of more than 100 nm. Such a thickness is likely to be fully excited by the hot electrons. Furthermore, one remarks that the travel time of hot electrons having a typical energy of 100 keV is less than 1 fs.

A different setup is shown in Figure 10. This geometry could be adapted to the case where the material to be studied has a too large $K\alpha$ wavelength to be diffracted by its own interplanar spacings ($\sin\theta = \frac{\lambda}{2d} > 1$). The idea is to use a target layer giving a shorter $K\alpha$ wavelength and to observe the sample in transmission. This is the essence of the transmission Kossel diffraction.⁵⁷ Here, the short and intense laser beam interacts with a high- Z (with respect to the sample) solid target to produce the short burst of hot electrons and the corresponding $K\alpha$ radiation. Its thickness is typically of the order of 1 μm , i.e. a compromise between hot electron transport, $K\alpha$ production and reabsorption. Behind this target is placed the sample to be analyzed and submitted to this $K\alpha$ radiation flux. In situations where thermodynamics of the sample must be adequately prepared by another *pump* laser, its thickness cannot go over about 100 nm for reasons given above. These two layers can conveniently be deposited on a substrate (glass) which is supposed to be transparent

both to the *pump* laser (of low intensity) and to the $K\alpha$ radiation (hard x-rays). One notes that in geometry, the $K\alpha$ emitting layer prevents also a significant perturbation of the sample by the hot electrons.

In both schemes, the angle of incidence between the high intensity laser and the target matters since mechanisms responsible of the hot electron production depend on it. However, for a given choice of this angle, one does not expect a significant change of the hot electron production over an angular interval of less one degree around this angle. If one chooses to keep position of the detector constant and to vary the angle of the target, this small interval is more than enough for the complete recording of a Kossel pattern emitted by a crystal material (see Figs. 3-6).

V. CONCLUSION

Time-resolved Kossel Diffraction has been shown to be a potential interesting technique for providing information on the structural order in a material. The observation of Kossel features around the Bragg angle is a signature of the periodic arrangement of atoms in a material. The method consists in performing an angular scan of the $K\alpha$ fluorescence emission induced by energetic particles (electrons, photons) crossing and ionizing inner-shells in a given material. As an alternative to XFEL photon bursts, the interaction of a short and intense laser pulse with a solid may provide short bursts of energetic electrons of about a few tens of fs which, through the observation of Kossel features, could permit to follow the structural dynamics in a well-prepared sample (at an earlier time than the source) provided that this material evolution is larger than about 0.1 to 1 ps. Such studies require to vary the delay between the source of hot electrons (i.e. the intense laser pulse) and the pump preparing the sample. This approach could be a new tool to get information concerning the characteristic evolution times of the structural order in a material previously excited by some external mean. While there is a lot of work to be done to master the Kossel pattern detection in extreme conditions, let emphasize again the possibility of phase retrieval with this technique. This unique aspect makes the ultrafast Kossel diffraction worth examining.

ACKNOWLEDGMENTS

The author thanks Philippe Jonnard and Jean-Michel André (LCPMR, Sorbonne Univ.) as well as Marc Sentis, Raphaël Clady and Olivier Uteza (LP3, Aix-Marseille Univ.) for helpful

discussions or comments especially about present experimental capabilities.

REFERENCES

- ¹T. Elsaesser and M. Woerner, "Perspective: Structural dynamics in condensed matter mapped by femtosecond x-ray diffraction", *J. Chem. Phys.* **140**, 020901 (2014).
- ²F. Dorchies and V. Recoules, "Non-equilibrium solid-to-plasma transition dynamics using XANES diagnostic", *Phys. Rep.* **657**, 1 (2016).
- ³A. Rousse, C. Rischel and J.C. Gauthier, "Femtosecond x-ray crystallography", *Rev. Mod. Phys.* **73**, 17 (2001).
- ⁴K. Sokolowski-Tinten, C. Blome, J. Blums et al, "Femtosecond X-ray measurement of coherent lattice vibrations near the Lindemann stability limit", *Nature* **422**, 287 (2003).
- ⁵M. Bargheer, N. Zhavoronkov, Y. Gritsai et al, "Coherent Atomic Motions in a Nanostructure Studied by Femtosecond X-ray Diffraction", *Science* **306**, 1771 (2004).
- ⁶A.M. Lindenberg, "Atomic-Scale Visualization of Inertial Dynamics", *Science* **308**, 392 (2005).
- ⁷D.M Fritz, D.A Reis, B. Adams et al, "Ultrafast Bond Softening in Bismuth: Mapping a Solid's Interatomic Potential with X-rays", *Science* **315**, 633 (2007).
- ⁸P. Beaud, S. L. Johnson, A. Streun et al, "Spatiotemporal Stability of a Femtosecond Hard X-Ray Undulator Source Studied by Control of Coherent Optical Phonons", *Phys. Rev. Lett.* **99**, 174801 (2007).
- ⁹Y. Azamoum, R. Clady, A. Ferré, M. Gambari, O. Utéza and M. Sentis, "High photon flux $K\alpha$ Mo x-ray source driven by a multi-terawatt femtosecond laser at 100 Hz ", *Optics Letters* **43**, 3574 (2018).
- ¹⁰M. Afshari, P. Krumei, D. Menn et al, "Time-resolved diffraction with an optimized short pulse laser plasma X-ray source", *Struct. Dyn.* **7**, 014301 (2020).
- ¹¹Marcel Holtz, Christoph Hauf, Jannick Weisshaupt et al, "Towards shot-noise limited diffraction experiments with table-top femtosecond hard x-ray sources", *Struct. Dyn.* **4**, 054304 (2017).
- ¹²P. Glatzel and U. Bergmann, "High resolution 1s core hole X-ray spectroscopy in 3d transition metal complexes", *Coord. Chem. Rev.* **249**, 65 (2005).
- ¹³W. Kossel, V. Loeck and H. Voges, "Die Richtungsverteilung der in einem Kristall entstandenen charakteristischen Röntgenstrahlung", *Z. Physik* **94**, 139 (1935).
- ¹⁴T. Gog, D. Bahr and G. Materlink, "Kossel diffraction in perfect crystals: X-ray standing waves in reverse", *Phys. Rev. B* **51**, 6761 (1995).
- ¹⁵J.T. Hutton, G.T. Trammell, and J.P. Hannon, "Determining the phase of the structure factor by

- Kossel cone analysis with the use of synchrotron radiation", *Phys. Rev. B* **31**, 743 (1985).
- ¹⁶G. Bortel, G. Faigel, M. Tegze and A. Chumakov, "Measurement of synchrotron-radiation-excited Kossel patterns", *J. Synchrotron Rad.* **23**, 214 (2016).
- ¹⁷G. Faigel, G. Bortel and M. Tegze, "Experimental phase determination of the structure factor from Kossel line profile", *Sci. Rep.* **6**, 22904 (2016).
- ¹⁸D.V. Novikov, B. Adams, T. Hiort et al, "X-ray Holography for Structural Imaging", *J. Synchrotron Rad.* **5**, 315 (1998).
- ¹⁹B. Adams, D.V. Novokov, T. Hiort, G. Materlik and E. Kossel, "Atomic holography with x-rays", *Phys. Rev. B* **57**, 7526 (1998).
- ²⁰A. Szöke, "X-ray and electron holography using a local reference beam", in *Short wavelength Coherent Radiation: Generation and Applications*, edited by T. Atwood and J. Boker, AIP Conf. Proc. No. 147 (AIP, New York, 1986), p. 361.
- ²¹M. Tegze and G. Faigel, "Atomic-Resolution X-ray holography", *Europhys. Lett.* **16**, 41 (1991).
- ²²M. Tegze and G. Faigel, "X-ray holography with atomic resolution", *Nature* **380**, 49 (1996).
- ²³K. Hayashi and P. Korecki, "X-ray Fluorescence Holography: Principles, Apparatus, and Applications", *J. Phys. Soc. Jpn* **87**, 061003 (2018).
- ²⁴W. Kossel, "Bemerkung zur scheinbaren selektiven Reflexion von Röntgenstrahlen an Kristallen", *Z. Physik* **23**, 278 (1924).
- ²⁵E. Langer and S. Däbritz, "75 years of Kossel patterns - past and future", *IOP Conf. Ser.: Mater. Sci. Eng.* **7**, 01215 (2010).
- ²⁶J.-P. Chauvineau and S. Bridou, "Analyse angulaire de la fluorescence du fer dans une multicouche périodique Fe/C", *J. Phys. IV France* **6**, C7-53 (1996).
- ²⁷P. Jonnard, J.-M. André and C. Bonnelle, "Modulation of x-ray line intensity emitted by a periodic structure under electron excitation", *Appl. Phys. Lett.* **81**, 1524 (2002).
- ²⁸P. Jonnard, J.-M. André, C. Bonnelle, F. Bridou, and B. Pardo, "Soft-x-ray Kossel structures from W/C multilayers under various electron ionization conditions", *Phys. Rev. A* **68**, 032505 (2003).
- ²⁹K. Le Guen J.-M. André, M. Wu et al, "Kossel Effect in Periodic Multilayers", *J. Nanosci. Nanotechnol.* **19**, 593 (2019).
- ³⁰O. Peyrusse, P. Jonnard, K. Le Guen and J.-M. André, "X-ray emission from layered media irradiated by an x-ray free-electron laser", *Phys. Rev. A* **101**, 013818 (2020).
- ³¹M. Sanchez del Rio, N. Perez-Bocanegra, X. Shi, V. Honkimäki and L. Zhang, "Simulation of

- X-ray diffraction profiles for bent anisotropic crystals", *J. Appl. Cryst.* **48**, 477 (2015).
- ³²M. Sanchez del Rio and R. J. Dejus, "Status of XOP: an x-ray optics software toolkit", *SPIE Proceedings* **5536**, 171 (2004).
- ³³M. Sanchez del Rio and R. J. Dejus, "XOP v2.4: recent developments of the x-ray optics software toolkit", *SPIE Proceedings* **8141**, 814115 (2011).
- ³⁴W. Schülke and O. Brümmer, "Vergleichende Untersuchungen von Interferenzen bei kohärenter und inkohärenter Lage der Röntgen-Strahlenquelle zum Kristallgitter", *Z. Naturforsch A* **17**, 208 (1962).
- ³⁵M. Born and E. Wolf, *Principles of Optics* (Pergamon, New-York, 1975).
- ³⁶O. Peyrusse, J.-M. André, P. Jonnard, and J. Gaudin, "Modeling of the interaction of an x-ray free-electron laser with large finite samples", *Phys. Rev. E* **96**, 043205 (2017).
- ³⁷C.L. Leakeas and E.W. Larsen, "Generalized Fokker-Planck Approximations of Particle Transport with Highly Forward-Peaked Scattering", *Nucl. Sci. Eng* **137**, 236 (2001).
- ³⁸<http://physics.nist.gov/PhysRefData/Star/Text/ESTAR.html>
- ³⁹L. Volpe, D Batani, A Morace and J.J. Santos, "Collisional and collective effects in two dimensional model for fast-electron transport in refluxing regime", *Phys. Plasmas* **20**, 013104 (2013).
- ⁴⁰S.C. Wilks, W. L. Kruer, M. Tabak and A. B. Langdon, "Absorption of ultra-intense laser pulses", *Phys. Rev. Lett.* **69**, 1383 (1992).
- ⁴¹M. Sherlock, "Universal scaling of the electron distribution function in one-dimensional simulations of relativistic laser-plasma interactions", *Phys. Plasmas* **16**, 103101 (2009).
- ⁴²J. Yu, Z. Jiang, J.C. Kieffer and A. Krol, "Hard x-ray emission in high intensity femtosecond laser-target interaction", *Phys. Plasmas* **6**, 1318 (1999).
- ⁴³J. R. Davies, R. Betti, P. M. Nilson and A. A. Solodov, "Copper K-shell emission cross sections for laser-solid experiments", *Phys. Plasmas*, **20**, 083118 (2013).
- ⁴⁴C. Hombourger, "An empirical expression for K-shell ionization cross section by electron impact", *J. Phys. B* **31**, 3693 (1998).
- ⁴⁵H. Sorum and J. Bremer, "High-resolution studies of the K emission spectra of nickel", *J. Phys. F* **12**, 2721 (1982).
- ⁴⁶Marcus H. Mendenhall, Lawrence T. Hudson, Csilla I Szabo, Albert Henins and James P. Cline, "The molybdenum K-shell emission spectrum", *J. Phys. B* **52**, 215004 (2019).
- ⁴⁷S.L. Johnson, P. Beaud, C.J. Milne et al, "Nanoscale Depth-Resolved Coherent Femtosecond Motion in Laser-Excited Bismuth", *Phys. Rev. Lett.*, **100**, 155501 (2008).

- ⁴⁸S. Pal and R.P. Gupta, "Phonon dispersion relations in nickel", *Solid State Comm.* **4**, 83 (1966).
- ⁴⁹M. Nicoul, U. Shymanovich, A. Tarasevitch, D. von der Linde and K. Sokolowski-Tinten, "Picosecond acoustic response of a laser-heated gold-film studied with time-resolved x-ray diffraction", *Appl. Phys. Lett.* **98**, 191902 (2011).
- ⁵⁰M. Först and T. Dekorsy, in *Coherent Vibrational Dynamics* edited by S. DeSilvestri, G. Cerullo and G. Lanzano (CRC Press, Taylor and Francis Group, London, 2008), p 129.
- ⁵¹"Layer specific observation of slow thermal equilibration in ultrathin metallic nanostructures by femtosecond X-ray diffraction", J. Pudell, A.A. Maznev, M. Herzog et al, *Nat. comm.* **9**, 3335 (2018).
- ⁵²V. Recoules, J. Clérouin, G. Zérah, P.M. Anglade and S. Mazevet, "Effect of intense laser irradiation of the lattice stability of semiconductors and metals", *Phys. Rev. Lett.* **96**, 055503 (2006).
- ⁵³S.L. Daraszewicz, Y. Giret, N. Naruse et al, "Structural dynamics of laser-irradiated gold nanofilms", *Phys. Rev. B* **88**, 184101 (2013).
- ⁵⁴Z. Lin, L.V. Zhigilei, and V. Celli, "Electron-phonon coupling and electron heat capacity of metals under conditions of strong electron-phonon nonequilibrium", *Phys. Rev. B* **77**, 075133 (2008).
- ⁵⁵M. Gambari, R. Clady, L. Videau et al, "Size broadening investigation of $K\alpha$ x-ray source produced by high intensity laser pulses", *Scientific Reports* **11**, 23318 (2021).
- ⁵⁶C. Fourment, N. Arazam, C. Bonte et al, "Broadband, high dynamics and high resolution charge coupled device-based spectrometer in dynamic mode for multi-keV repetitive x-ray sources", *Rev. Sci. Inst.* **80**, 083505 (2009).
- ⁵⁷S.P. Bellier and R.D. Doherty, "The structure of deformed aluminium and its recrystallization - Investigations with transmission Kossel diffraction", *Acta Metallurgica* **25**, 521 (1977).